A Multiresolution Approach to the Extraction of the Pyloric Rhythm

Filipa dos Santos 1, Peter Andras 2, and KP Lam 3
School of Computing and Mathematics
Keele University
Newcastle-under-Lyme, UK
Email: f.dos.santos@keele.ac.uk

***Abstract*—This paper describes our work toward the development of a computationally robust methodology to identify the pyloric neurons in the stomatogastric ganglion of *Cancer pagurus* using voltage-sensitive dye imaging. The multi-resolution signal decomposition procedure constructed using the sequential Singular Spectrum Analysis approach to isolate the pyloric rhythm from optical recordings of dyed live cells is presented. Early results suggest that the developed procedure offers a demonstrably reliable way to extract the rhythm from the recording data of these cells.**

***Keywords*— multiresolution signal processing, optical recording, singular spectrum analysis, stomatogastric ganglion, voltage sensitive dye**

I. Introduction

The pyloric rhythm network is one of the most well-known central pattern generators (CPG) in the crustacean stomatogastric ganglion (STG), which controls the pylorus or pyloric filter of the decapod crustaceans to facilitate mixing of food particles resultant from the gastric milling process. The rhythm has a spontaneous activity that can be kept active *in vitro* for up to two weeks [1], [2]. Specifically, it is a relatively strong and continuous tri-phasic rhythm which is characterised by a motor pattern frequency of typically 1Hz, although it varies between 0.3Hz and 3Hz [3], [4].

This paper describes our work toward the development of a reliable and computationally robust methodology to identify the neurons contributing to the pyloric rhythm by analysing voltage-sensitive dye imaging (VSDi) data recorded from the crab STG. Briefly, VSDi is an experimental technique adopted in the past few decades to facilitate both *in vivo* and *in vitro* studies of many different biological tissues, including the analysis of small invertebrate neural circuits [5], [6]. In particular, fast response voltage-sensitive dyes (VSDs) have been used as chemical probes that attach to cell membranes and change their fluorescence or absorbance, in response to electrical field changes registered in the transmembrane potential [7].

In recent years, VSDi has been used successfully in the stomatogastric nervous system (STNS) of decapod crustaceans [8]–[11] offering a promising approach to investigate multi-neuron dynamics and the emergence of network scale functionality in neural systems. Previous results concerning the identification of neurons using VSDi data rely on the so-called *event-triggered averaging* procedure, which has been applied to the data over fixed windows of pyloric cycles. From a signal analysis viewpoint, such a low-pass filtering procedure does not only remove noise and small scale fluctuations in the data, but also smooths sharp changes associated with the relatively large amplitude and coherent structures of the characterising spikes observable from the different types of neurons, making the precise identification of cells much more difficult. More importantly, the problem is compounded by the relatively low yield of the potential-dependent fluorescence change (2-10%/100mV)[1], and thus the typically poor signal-to-noise ratio (SNR), achieved by the fast response VSD (Di-4-ANEPPS) that was adopted in our studies.

The organisation of this paper is as follows. Section II describes the experimental setup which outlines the concerned procedures for the optical recording experiments carried out for our studies and the subsequent data extraction/collection. The description of the data/signal processing procedure from which the collected data are analysed, including in particular the multiresolution approach based on the sequential Singular Spectrum Analysis (s-SSA) to extract pyloric rhythm is presented in section III. Preliminary results are discussed in section IV, which is followed by the concluding remarks and future work presented in section V.

II. Experimental setup

A. Dissection

Adult *Cancer pagurus* were obtained from Hodgkinson Fresh Fish, Manchester, and kept in artificial seawater tanks (red sea salt, Red Sea) at 12-14°C with 12h light-dark cycle[2]. The crabs were anaesthetised before the dissection by placing in an ice bucket for 20-30min. The dissection of the STNS was performed using the protocol described by [12]. Desheathing of the STG was executed to allow better penetration of the dye. The STNS was pinned down in a silicone elastomer-lined (ELASTOSIL RT-601, Wacker, Munich, Germany) petri dish.

[1] https://www.thermofisher.com/order/catalog/product/D1199

[2] All experiments were carried out in accordance with the European Communities Council Directive of 24th November 1986 (86/609/EEC).

The saline solution was changed every 10min to keep a constant temperature of 11-13°C and the pH 7.4-7.6. The saline solution consisted of mMol l^{-1}: NaCl, 440; $MgCl_2$, 26; $CaCl_2$, 13; KCl, 11; trisma base, 10; maleic acid, 5.

B. Extracellular and image recording

Standard electrophysiology methods were performed [13]–[15]. Petroleum jelly well was built around the lateroventral nerve (lvn) to isolate the section and to enable the analogue signal to be recorded. One stainless steel electrode wire was placed inside this well, and the other in the bath as a reference. The differential signal was recorded, filtered and amplified by an AC differential amplifier (A-M Systems model 1700) and converted using Spike2 v8.07 (Cambridge Electronic Design, Cambridge, UK). The image was recorded using the MiCAM02 imaging system (SciMedia Ltd., Tokyo, Japan) using the analogue output as described above**.** A high-resolution (192x128) image was first taken for each experiment to help (better) identify the individual cells within the field of view of the microscope from a series of low resolution (48x32) coregistered images recorded over the course of a recording; see further description in *Data Collection* below. These low-resolution images form a (3-D) image stack which, for the purpose of our studies, provides a series of 21,840 images sampled over the course of a recording, offering a temporal resolution of 1.5ms. The biological sample (or prep) was seating on a standard upright fluorescence microscope (BX51WI, Olympus Corporation, Tokyo, Japan) which is equipped with a 20x mounted objective (XLUMPLFL20xW, N.A. 0.95, WD 2.0mm; Olympus Corporation, Tokyo, Japan). The lighting was delivered from a 150W halogen light source (HL-151, Moritex Corporation, Tokyo, Japan) with a computer controlled shutter. A wide green excitation filter was used (480–550 nm, MSWG2, Olympus Corp., Tokyo, Japan). Light levels were adjusted to minimise potential phototoxic damage.

C. Dye preparation – Di-4-ANEPPS

Di-4-ANEPPS (Cambridge Bioscience, Cambridge, UK) used by bath application on the STG surrounded by a petroleum jelly-well. The dye was kept in stock solution – 5mg di-4-ANEPPS dissolved in 1ml Pluronic F-127 (20% solution in DMSO). On the day of each experiment, 10µl of the stock solution was mixed with 500µl of saline. The dyed prep was then left in the fridge for approximately 20 minutes. This done, the petroleum jelly well from around the STG was removed, and the dye was washed out using a saline flow.

D. Data collection

The data obtained from the optical recordings as described above was extracted using the BVAna imaging software (SciMedia Ltd., Tokyo, Japan)**,** which exports the data from the 3-D image stack stored for each recording into CSV formatted spreadsheets.

Here, a number of pixels were meticulously chosen from each identifiable cell, collated as the distinct region of interest (ROI), within the field-of-view of the high resolution (2-D) image described above; see Fig. 1. These pixels were then mapped to the corresponding pixels in the (low-resolution) image stack, from which values of the selected pixels were extracted in the form of 1-D time/signal sequences from successive images of the 3-D stack; see Fig. 2 for illustration. This process is repeated for areas covering all other cells, or ROIs, that have been identified, including importantly the *neuropil*.

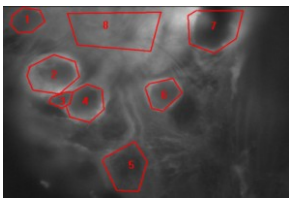

Fig. 1. An example of a high-resolution image from which the individual cells/ROIs (numbered 1-7) were identified. ROI 8 corresponds to the neuropil.

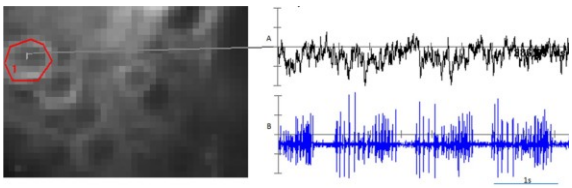

Fig. 2. The corresponding low-resolution image/stack (see figure 1) where a pixel of the identified ROI is selected, with the extracted (1-D) time sequence shown in A (right). The simultaneously recorded lvn signal is also shown in B (right) for reference.

It is noted that the number of pixels extracted from each cell varies, depending on the size of the visibly identifiable area of the cell/neuron.

III. Signal/Data Analysis

A principal challenge in estimating the pyloric rhythm from recorded data is the relatively poor SNRs achieved by the VSDs. This is illustrated in Fig. 3, where the power spectrum of the time sequence is also depicted in (B). The latter figure reveals several notable features of the collated time sequences for the individual cells/ROIs. First, the power spectrum was often dominated by some slow varying trends that peaked at a frequency of 0.06Hz[3], significantly lower than the extracted pyloric rhythm (at 0.73Hz). This is evident in Fig. 3(A) where the mean-shifted sequence slightly fluctuates between the time-axis. Second, in addition to highly correlated (sinusoidal) signal components, there were other bandlimited (noise) processes which seemed unrelated to the pyloric rhythm. Third, uncorrelated white noise which covered almost the entire spectrum (0 to 333Hz) was also present.

To address the above, spectral analysis methods based on singular-value or eigendecomposition that is generally known to provide good resolution and frequency estimation characteristics were chosen to identify and (subsequently) extract the pyloric rhythm. Such a signal decomposition approach is particularly effective in separating highly correlated signal components (e.g. sinusoidal or exponential), or other narrowband processes that are uncorrelated to white noise – except that the technique is much less effective at

[3] We note that this may correspond to an underlying gastric mill rhythm activity for which the typical frequency range is 0.05 – 0.2 Hz.

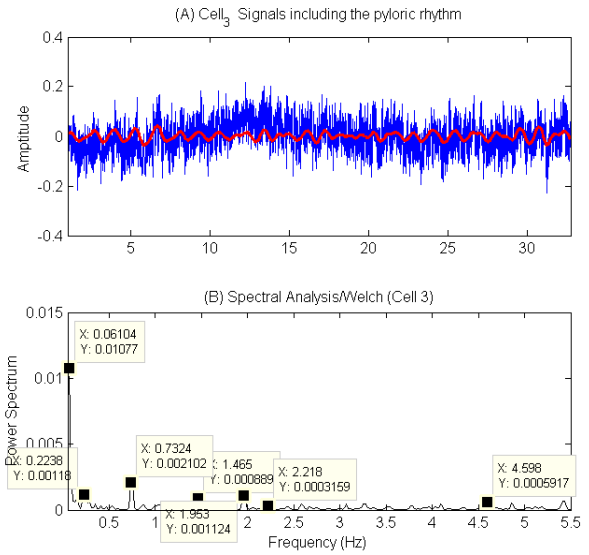

Fig. 3. (A) The time sequence shown in blue represents the mean-shifted signal 3 (as ensemble average) obtained from cell 3 is overlaid with the extracted pyloric rhythm (in red). (B) The power spectrum computed for the time sequence depicted in (A). The pyloric rhythm corresponds to a frequency of 0.7324 Hz in this experiment.

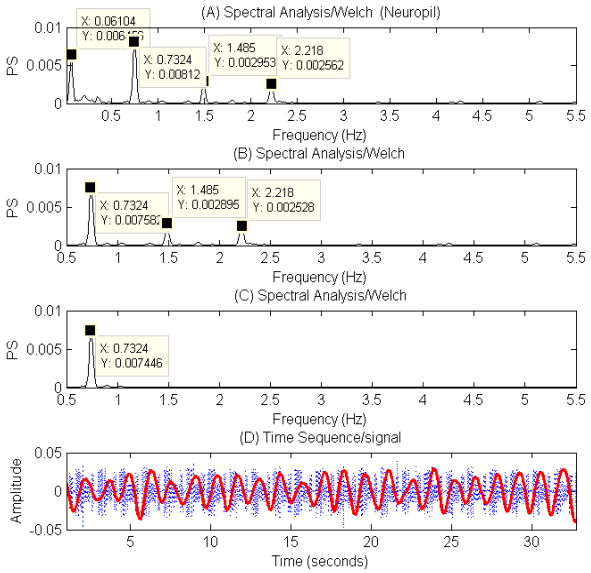

Fig. 4. (A) The computed power spectrum (PS) for the Neuropil. (B) The PS computed for the extracted signal/components following the 1st stage of the s-SSA procedure. (C) As (B), the extracted component after the 2-stage s-SSA procedure. (D) The extracted neuropil signal/PR shown in red is compared with the analogue signal (blue).

separating broadband processes from such noise as they are generally unstructured. Here, we adopt the widely used technique of singular spectrum analysis (SSA) that has found applications in a broad range of tasks in classic time-series analysis, multivariate statistics, dynamical systems, signal processing and, latterly, biomedical engineering [16]–[18].

Broadly speaking, the technique seeks to decompose the original signal into two subspaces; (i) a signal consisting of the mixture of a small number of independent and interpretable components, and (ii) a structureless noise. More specifically, a multiresolution procedure similar to the wavelet analysis of signals has been constructed using the so-called sequential SSA (s-SSA). By applying the basic SSA repeatedly with different parameters to the residuals from the previous analysis, the approach of the s-SSA was taken specifically to separate the pyloric rhythm from the original sequence that has shown to display a more complex form. Here, such a procedure was developed to resolve the mixing problem of signal components within the collated time sequences from each ROI, or formally, the problem of close singular values for weakly separate sequence components [17].

A. Neuropil

The multi-resolution procedure of the s-SSA was applied to the time sequences collated for the STG neuropil from the experiment. The reasons are twofold; firstly, it is known that recordings from the neuropil, a synaptically dense region in the nervous system composed of mostly axons, dendrites and glial cell processes, are dominated by the pyloric rhythm in the STG. As such, it can be used to provide a reference or ground truth to compare with the extracted signal/components from each cell. Secondly, the features obtained by studying the power spectrum can be used to help determine the parameters used with the s-SSA; namely, the choice of the initial window width (L). This is illustrated in Fig. 4(A), where the pyloric rhythm (PR) is clearly visible at 0.7324Hz.

Given the sampling rate R (= 1.5ms), this corresponds to a minimum window width (L_{min}) which can be computed as follows:

$$L_{min} = (1/PR) / R = (1/0.7324) /1.5 * 10^3 = 910. \quad (1)$$

Thus, L was set at 1000 for the first stage of the s-SSA procedure, and the resulting power spectrum (PS) of the separated signal is shown in Fig. 4(B). Here, it should be apparent that the slow varying trend that peaks at 0.06Hz and the (low frequency) noise present in the neighbourhoods leading up to the PR were completely removed.

At the second stage of the s-SSA whereby the PR was extracted, L was set to 1250 to afford the basic SSA scheme a finer spectral resolution. Here, it should be noted that the grouping and subsequently selection of the components generated by the SSA was guided by the scree-plot (not shown here) computed following its in-built eigenvalue decomposition procedure. The power spectrum of the computed PR following this final stage of the s-SSA procedure is given in Fig. 4(C), where it is shown that the PR was located accurately and practically free of noise. The analogue signal recorded from the lvn (blue) is included in Fig. 4(D), to help compare with and validate the extracted PR (red).

IV. Results and Discussions

The 2-stage s-SSA procedure was applied to the 16 cells recorded in our first experiment. The results are summarised in Table I, which includes the signal characteristics computed for

both the original and s-SSA extracted time sequences based on spectral analysis method used in the preceding section.

A few notes are in order. First, the PR was clearly present in some, but not all, of the cells (highlighted). This seems reasonable, as the number of neurons responsible for the characteristic triphase pattern of the PR is known to be comprised of 11 neurons; namely, 1 AB, 1 LP, 1 VD, 1 IC, 5 PY and 2 PD neurons [1], [2]. Also, pyloric timed modulations were also observed in some cases, suggesting the presence of the gastric mill network neurons. Second, some cells (2, 3, 7 & 15) showed a rhythm which is very close to the PR; although in all these cases, the PR (0.7324Hz) were also present in the spectrum as the 2nd largest component in the extracted time sequences. Therefore, it is likely that they are part of the pyloric cells. Third, the % separation displayed in column 6 represents the proportion of the signal power separated by the s-SSA from the original time sequence, (thus) demonstrating the effectiveness of the s-SSA procedure in terms of the PR extraction. Here, it is noted that, in most cases where the PR is detected, the percentage is over 85%. Last but not the least, the measured SNR (column 7) is relatively and consistently low, at approximately -20dB, which is in agreement with the specifications (2-10% change per 100mV) of the dye (Di-4-ANEPPS) used in the experiment.

Similar results were also achieved by the second experiment.

TABLE I. RESULTS OBTAINED FOR EXPERIMENT 1 (WITH 16 CELLS)

Cell ID	Original		s-SSA separation		% Sep	SNR (dB)	PR (Y/N)
	Fq(Hz)	*Amplitude*	*Fq(Hz)*	*Amplitude*			
1	0.8748	0.001298	0.8748	0.000273	21	-22	N
2	0.7528	0.002820	0.7528	0.002386	85	-17	Y
3	0.7528	0.002280	0.7528	0.001996	88	-19	Y
4	0.8748	0.000724	1.6070	0.000327	45	-23	N
5	0.7324	0.009484	0.7324	0.009219	97	-12	Y
6	0.7324	0.000716	0.7324	0.000660	92	-22	Y
7	0.7528	0.001771	0.7528	0.001701	96	-20	Y
8	2.7060	0.001231	1.6680	0.000425	34	-22	N
9	0.8952	0.000806	0.8952	0.000601	75	-22	N
10	0.7324	0.02247	0.7324	0.019510	87	-14	Y
11	0.8952	0.001380	0.8952	0.001050	76	-22	N
12	0.8952	0.002250	0.8952	0.001470	65	-20	N
13	0.7324	0.006267	0.7324	0.006103	97	-15	Y
14	0.7324	0.001472	0.7324	0.001356	92	-19	Y
15	0.7528	0.007351	0.7528	0.007045	96	-12	Y
16	1.0580	0.001790	0.8952	0.001561	87	-21	N

V. CONCLUSION AND FUTURE WORK

The PR extraction from pyloric neurons in the STG circuit of *Cancer pagurus* using the technique of VSDi with live cells is a complex signal processing task. To address the poor SNRs typically achieved by such dyes, a multiresolution signal decomposition procedure based on the s-SSA approach has been developed to reliably separate the pyloric rhythm from optical recordings of dyed live cells. In addition to the use of intracellular recordings of the participating neurons, to elicit the ultimate ground truth, work is currently underway to develop computationally tractable and biologically meaningful metrics that will identify from these images the neurons responsible for generating the extracted PR. This will permit us to employ two previously developed techniques; namely, spectral signature generator [19] and image pixel guided tours based on Independent Component Analysis [20].

REFERENCES

[1] M. P. Nusbaum and M. P. Beenhakker, "A small-systems approach to motor pattern generation," Nature, vol. 417, pp. 343–350, May 2002.

[2] E. Marder and D. Bucher, "Understanding circuit dynamics using the stomatogastric nervous system of lobsters and crabs," Annu. Rev. Physiol., vol. 69, pp. 13.1-13.26, September 2006.

[3] U. B. S. Hedrich, F. Diehl, and W. Stein, "Gastric and pyloric motor pattern control by a modulatory projection neuron in the intact crab Cancer pagurus," J. Neurophysiol., vol. 105, pp. 1671–1680, February 2011.

[4] C. Derby and M. Thiel, Nervous Systems and Control of Behavior (The Natural History of Crustacea), Volume 3. New York: Oxford University Press, 2014.

[5] S. Chemla and F. Chavane, "Voltage-sensitive dye imaging: Technique review and models," J. Physiol., vol. 104, pp. 40–50, 2010.

[6] E. S. Hill, A. M. Bruno, and W. N. Frost, "Recent developments in VSD imaging of small neuronal networks," Learn. Mem., vol. 21, pp. 499–505, September 2014.

[7] V. Tsytsarev, et al., "Recent progress in voltage-sensitive dye imaging for neuroscience," *J. Nanosci. Nanotechnol.*, vol. 14, no. 7, pp. 4733–4744, July 2014.

[8] W. Stein and P. Andras, "Light-induced effects of a fluorescent voltage-sensitive dye on neuronal activity in the crab Stomatogastric Ganglion," J. Neurosci. Methods, vol. 188, pp. 290–294, March 2010.

[9] W. Stein, C. Städele, and P. Andras, "Single-sweep voltage-sensitive dye imaging of interacting identified neurons," J. Neurosci. Methods, vol. 194, pp. 224–234, October 2011.

[10] C. Städele, P. Andras, and W. Stein, "Simultaneous measurement of membrane potential changes in multiple pattern generating neurons using voltage sensitive dye imaging," J. Neurosci. Methods, vol. 203, pp. 78–88, September 2012.

[11] S. Preuss and W. Stein, "Comparison of two voltage-sensitive dyes and their suitability for long-term imaging of neuronal activity," PLoS One, vol. 8, no. 10, pp. 1–13, October 2013.

[12] G. J. Gutierrez and R. G. Grashow, "Cancer borealis Stomatogastric Nervous System dissection," J. Vis. Exp., pp. 1–5, January 2009.

[13] M. Bartos and M. P. Nusbaum, "Intercircuit control of motor pattern modulation by presynaptic inhibition," J. Neurosci., vol. 17, no. 7, pp. 2247–2256, April 1997.

[14] D. M. Blitz and M. P. Nusbaum, "Motor pattern selection via inhibition of parallel pathways," J. Neurosci., vol. 17, no. 13, pp. 4965–4975, July 1997.

[15] W. Stein, C. R. Smarandache, M. Nickmann, and U. B. S. Hedrich, "Functional consequences of activity-dependent synaptic enhancement at a crustacean neuromuscular junction," J. Exp. Biol., vol. 209, pp. 1285–1300, January 2006.

[16] F. Ghaderi, H. R. Mohseni, and S. Sanei, "Localizing heart sounds in respiratory signals using singular spectrum analysis," IEEE Trans. Biomed. Eng., vol. 58, no. 12 PART 1, pp. 3360–3367, December 2011.

[17] N. Golyandina and A. Zhigljavsky, Singular Spectrum Analysis for Time Series. New York: Springer, 2013.

[18] K. P. Lam, K. P. Dempsey, D. J. Collins, and J. B. Richardson, "Monitoring stem cells in phase contrast imaging," 2016, p. 97110E.

[19] K. Lam, J. C. Austin, and C. R. Day, "A coarse-grained spectral signature generator," 2007, p. 63560S.

[20] K. Lam and R. Emery, "Image pixel guided tours: a software platform for non-destructive x-ray imaging," 2009, p. 72450N.